



Deep learning analysis and age prediction from shoeprints

Muhammad Hassan^a, Yan Wang^a, Di Wang^b, Daixi Li^c, Yanchun Liang^a, You Zhou^{a,e,*}, Dong Xu^{d,**}



^a College of Computer Science and Technology, Jilin University, Changchun, China

^b Joint NTU-UBC Research Centre of Excellence in Active Living for the Elderly, Nanyang Technological University, Singapore

^c CEO of Everspray Science and Technology Company Ltd., Dalian, China

^d Department of Electrical Engineering and Computer Science, Bond Life Sciences Center, University of Missouri, Columbia, MO, United States

^e Key Laboratory of Symbolic Computation and Knowledge Engineering of Ministry of Education, Jilin University, Changchun, China

ARTICLE INFO

Article history:

Received 3 April 2021

Received in revised form 26 August 2021

Accepted 27 August 2021

Available online 30 August 2021

Keywords:

Shoeprint

Gait-and-standing patterns

Aging

Age prediction

Deep learning

Pressure distribution

ABSTRACT

Human gaits are the patterns of limb movements which involve both the upper and lower body parts. These patterns in terms of step rate, gait speed, stance widening, stride, and bipedal forces are influenced by different factors including environmental (such as social, cultural, and behavioral traits) and physical changes (such as age and health status). These factors are reflected on the imprinted shoeprints generated with body forces, which in turn can be used to predict age, a problem not systematically addressed using any computational approach. We collected 100,000 shoeprints of subjects ranging from 7 to 80 years old and used the data to develop a deep learning end-to-end model ShoeNet to analyze age-related patterns and predict age. The model integrates various convolutional neural network models together using a skip mechanism to extract age-related features, especially in pressure and abrasion regions from pair-wise shoeprints. The results show that 40.23% of the subjects had prediction errors within 5-years of age and the prediction accuracy for gender/sex classification reached 86.07%. Interestingly, the age-related features mostly reside in the asymmetric differences between left and right shoeprints. The analysis also reveals interesting age-related and gender-related patterns in the pressure distributions on shoeprints; in particular, the pressure forces spread from the middle of the toe toward outside regions over age with gender-specific variations of forces on heel regions. Such statistics provide insight into new methods for forensic investigations, medical studies of gait pattern disorders, biometrics, and sport studies.

© 2021 The Author(s). Published by Elsevier B.V.

CC_BY_NC_ND_4.0

1. Introduction

A shoeprint is the impression mark made by the contact of footwear tread with the ground surface [1]. Such impressions in the digitized format can be captured from pressed regions of footwear in a standing or walking position [2,3]. Retrieving shoeprints is a challenging computer vision problem given various factors such as textures, designs, manufacture models and wear-effects [4]. Many processing methods have been applied for retrieving shoeprints,

including manual [5], semi-automated [6,7], and automated [8,9] approaches, especially machine-learning [10–12] based automated methods. Recently, deep learning methods have been applied in processing, which include features extraction, reconstruction and investigation of shoeprints; furthermore, these methods have achieved some good results [10–13] leading to more extensive studies on shoeprints matching [14], recognition [15], and reconstruction [11,16]. Some of these studies are carried out for crime-scene investigation, such as forensic podiatry [10,14,17–19] while others focus on biological trait examination and investigation, such as stature estimation [20], gender prediction [19,21,22] and body morphology examination [23]. Unlike other biometric modalities, such as fingerprints, palm-prints, and retina prints, shoeprints have inconsistent patterns, shape, and appearance, except for wear-effects. Such effects are associated with distinct traits including gait patterns, personality, mood, social and cultural variances, age, and gender [24–27] which provides a basis for crime-scene investigations, perpetrator gait analyses, and sport and health examinations.

* Corresponding author at: College of Computer Science and Technology, Jilin University, Changchun, China.

** Corresponding author.

E-mail addresses: mhassandev@gmail.com, hassan2117@mails.jlu.edu.cn (M. Hassan), wy6868@jlu.edu.cn (Y. Wang), WangDi@ntu.edu.sg (D. Wang), lidaxi@everspry.com (D. Li), ycliang@jlu.edu.cn (Y. Liang), zyou@jlu.edu.cn (Y. Zhou), xudong@missouri.edu (D. Xu).

The most relevant biological profile to forensic investigation are gender/sex, age, body morphology, ancestry, etc which rely on skeletal materials [28–30]. Among biological profiles, age is a common trait that can be reflected in shoeprints. In contrast to age predictions based on other human traits including facial images [31,32] brain MRI and EEG [33–35], DNA [36] and gait patterns [37,38], age prediction from shoeprints is more challenging due to image noises, varying patterns, and shoe designs. Most importantly, wear-effects on shoeprints are influenced by various biomechanics such as the weight, gait patterns, environmental factors, personality, and tread materials of the shoes [11]. Hence, although forensic experts often estimate the age of the shoe owners from shoeprints empirically, no systematic computational method has been developed to predict age based on shoeprints. To predict age based on shoeprints systematically, it is essential to study their relationships as shown by age, gait, standing patterns, and shoeprints. The estimation of age and sex from shoeprint impressions ease the investigation and examination processes. Likewise, shoeprints can be used to narrow down a large pool of suspects to a smaller pool of suspects. Based on our study, prior to other biological traits investigation in a large scale population, the investigators may first determine the suspects' sex-category (i.e., either male or female) and then estimate the age-group (e.g., 31- to 40-year-old), which will reduce the population size. Therefore, shoeprint-based (i.e, age, gender/sex¹) classification and age prediction assist the forensic investigation and examination processes. Notably, this paper present the first study to estimate human traits using a machine intelligence approach. Contrary to morphological features extraction as carried conventionally [20–22,19], the model will consider wear-and-tear effects, asymmetric difference, and relate biomechanics forces from pair of large size shoeprint dataset. In prior studies [22,28], morphological features (i.e., length, width) and dimension have been used for biological profile estimation (sexual dimorphism, stature, and age). In the study of [39], the human body stature (height) is associated with the dimensions of foot and shoeprint. However, these studies do not exploit biological profile (age, gender) estimation especially using machine/deep learning approach. Moreover, it is very hard and expensive to train a high-level expertise to delicately estimate age and gender from shoeprints. To the best of our knowledge, this is the first systematic approach to estimate human age and gender from a large-scale shoeprint dataset using a machine learning algorithm. By adopting this model, we automate the age and gender estimation up to an encouraging level of precision, which comes along with the benefits of cost-effectiveness, better scalability, reliable decision support, and so on.

Aging is significantly associated with gait patterns in the capacity of stances, bipedal floor contact, step length, posture stooping during walking, gender and ethnicity [38,40–43]. It is known that gait speed [44], step rate [45], stance and gait-based widening [38] are related to aging [20,46]. Some studies have reported that in normal walking, elder people (age > 65 years) prefer 41% wider steps than younger subjects (age < 30 years) [27,37]. Furthermore, such variational effects are also reflected in the pressure distributions of the footwear as muscles recalibrate themselves over age. The energy cost for muscle movements during walking is high in children and steadily decreases over age [47,48] which can be reflected in the imprinted shoeprints of healthy subjects [37,42,49]. The wear-effects with natural erosion on shoeprints have the potential to be used for predicting age by involving distinct contact regions of the footwear [49–52]. Thus, our study systematically associates the relationship among aging, gait pattern, and shoeprints.

In this study, we explored and analyzed the relationship between aging and shoeprints and used the relationship to predict age from

shoeprints using a deep learning approach, as shown in Fig. 1. This study aims to estimate age and gender from digitally captured shoeprints via a machine learning approach. The findings in terms of age and sex will assist investigation stage by narrowing down a large scale of population to a smaller pool of suspects. Our contributions to this new research area include: 1) To the best of our knowledge, this study represents the first effort to systematically explore the relationship among aging, gait pattern, and shoeprints. 2) We collected 100,000 images featuring 50,000 subjects between the ages of 7 and 80 years old thereby providing a large-scale annotated shoeprint dataset for the research community to use in related studies. 3) We proposed a convolution neural network (CNN) adapted model named ShoeNet based on the comparative studies of different deep learning approaches to predict age, and 4) we statistically analyzed group-wise pressure distributions based on age. Our findings successfully revealed the association of biological profiles with the wear-effects reflected on shoeprints, which can be used for biological profile estimations, forensic investigations, and examining sports and health activities.

2. Methodology

2.1. Datasets acquisition and generation

We collected shoeprints by having subjects step on the strip of the Everspy Outsole Scanner (EverOS V2.0) acquisition system (Fig. 2), over a period of two years (2017–2018). It is an intelligent footprint terminal system which collects footprint and shoeprint samples using optical-array sensors. The footprint terminal system also generates corresponding standard shoeprint pattern images in digitalized form. The hardware structure is 402 mm long × 315 mm wide × 152 mm-high with a collection scope of 350 mm × 150 mm, having a USB-3.0 interface and output images in 300-DPI (Supplementary Fig. S1). The equipment can preprocess the acquired image by removing the background noise. Prior to training a deep network model, the acquired images were pre-processed by resizing each of them into the same dimensions (224 H × 112 W), converting each image into a hue-saturation-value (HSV) format and masking the strip using a threshold value. To train the ShoeNet model, we flipped the images to the natural orientation and discarded poor-quality images manually. In most cases, a network model requires a balance dataset; hence, the number of samples per age range varies significantly so that the augmentation was performed to balance the sample distribution and increase the diversity of images per age range by providing an extensive amount of refined data for training deep-learning models. The augmentation operations included Gaussian-noise, flipping (left-to-right), rotation, and cropping shoeprints.

There are 100,000 images in total obtained from 50,000 subjects ranging from age 7-to- 80. Each subject has two (left, right) shoeprint images. Prior to data collection, relevant ethical approval, numbered SY20210620-1, was obtained considering the age of subjects. Shoeprints acquisition from subjects in the minor ages were carried out in the presence of at least one guardian by following all the ethical rules. There is no harm imposed to the recruited participants nor personal identifiable information are collected. To the best of our knowledge, this is the largest scale dataset of shoeprints with annotated information of age, gender, height and weight as well as rulers embedded on one side of each shoeprint [17]. A list of data generation versions was applied to facilitate a wide range of deep learning practices in terms of a biological profile estimation (Fig. 2(a)). The main features of the dataset versions are listed in Table 1 and are described as follows: Dataset-A contains the original images with two (left & right) shoeprints for each subject (Fig. 2). The number of samples distribution for male and female in Dataset-A are 61,437 and 12,693, respectively. To comprehend and process

¹ By gender we means male and female.

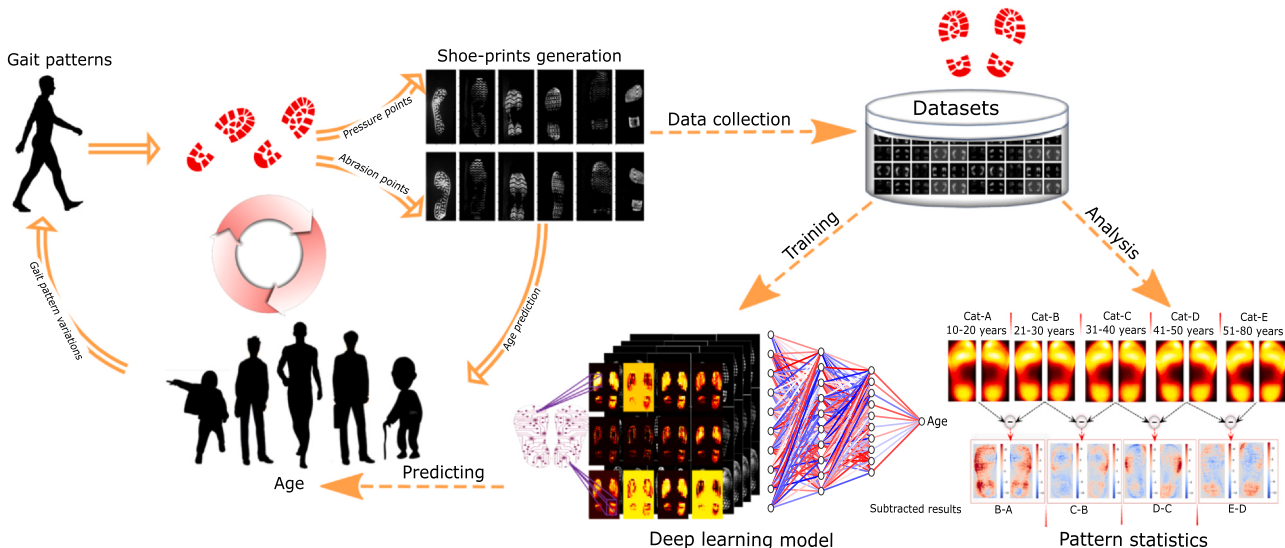


Fig. 1. The workflow of this study for age prediction and analysis from shoeprints. The relationship (O-shape) among aging, gait/standing patterns, and shoeprints. Based on the data collection for training deep learning models, the age prediction model is trained. The core model is ShoeNet to predict age. Variations of pressure forces on shoeprints versus age progression as well as the plots of region-wise trends are obtained from the data.

Table 1
Seven dataset versions.

Dataset	No. of Samples	Dimension (H x W)	LSO	RSO	BLR	Ruler	Gender	Description
Dataset-A	100,000	224x112	-	-	✓	✓	-	Original dataset
Dataset-B	100,000	224x112	-	-	✓	-	-	Ruler-less, flipped
Dataset-C	42,890	224x112	✓	-	-	-	-	Left shoeprints
Dataset-D	42,890	224x112	-	✓	-	-	-	Right shoeprints
Dataset-E	42,890	224x224	-	-	✓	-	-	Pairwise
Dataset-F	60,482	224x112	-	-	✓	-	✓	Gender dataset
Dataset-G	151,000	224x112	-	-	✓	-	-	Balance dataset

Left shoeprints only – LSO, Right only – RSO, Both left-and-Right – BLR. The list of dataset versions was generated to practice a wide range of experiments related to age estimation. Each dataset is described by number of samples, image-dimensions, whether including left or right or both shoeprints, scale, and gender information. The checkmarks (✓) exhibit the existence of the features. Dataset-C and Dataset-D were used for the comparative study of custom modalities, while standard modalities and ShoeNet were trained on Dataset-G. Dataset-G was augmented to balance the number of samples per age period. Similarly, Dataset-F was used for shoeprint-based gender classification and analysis.

conveniently, we grouped the subjects into eleven age-groups start from 7 to 18 (1459 samples per age-group), 19–25 year (8637 samples) to 65–80 year (364 samples). Similarly, we also illustrated the male and female subjects distributions in each age group. The detailed statistical description for samples distribution is shown in [Supplementary Table S1](#). For Dataset-B, the ruler/scale attached to every image, to measure the morphological features, was discarded without removing any information of the shoeprints. In some cases, the ruler is not perfectly aligned against the shoeprint images which may diverge the training process of the deep learning model.

To further refine, all the shoeprints were aligned manually in natural order as pairwise-shoeprints worn by humans. To train a reliable deep model, it is critical to feed the data with insightful features and to achieve at least the average performance [53,54]. Poor quality images were discarded manually after proper training by the experts in the machine learning. Two main criteria were setup for discarding poor quality images: 1) the cut-off was defined as the images that even an experienced human expert cannot make a viable estimation as shoeprint, and 2) above 75% regions of the shoeprints are abrasive and missed. Hence, we set the quality evaluation threshold as 75%, which means if an image has 75% or more absence of positive pixels (the background is regarded as negative), this image is deemed as of poor quality and is discarded from the training dataset. The subjective method is followed for discarding because the deep learning models imitate human neural system to learn knowledge from data. Still, our collected dataset contains shoeprint images which are quite similar in various aspects to the

image often found in crime scenes. For instance, the collected dataset contains abrasive, scratched, noisy, partial, and incomplete shoeprint images which show similarities with the foot impressions found in real scenarios. Thus, by training the proposed model with the collected dataset, it may provide great help in real forensic investigations.

Dataset-C solely holds the left shoeprints only, while Dataset-D conversely holds the right shoeprints only. Dataset-E integrates left & right shoeprints into a single pair-wise shoeprint ([Fig. 2](#)). Dataset-F is comprised of shoeprints separated for gender-sex to train models for male and female classification and age estimation. By gender, we mean the biological sex that includes males and females. The gender information is declared by the subjects themselves during data collection. For brevity, we use gender in this study to represent biological sex. To classify gender, we need a balanced dataset; however, the existing dataset is imbalanced in the number of male-and-female samples. For this purpose, we performed augmentation by the inclusion of Gaussian-noise, rotating and cropping to balance the number of samples between males and females. The overall statistics, including the original dataset, before and after augmentation, training, validation and testing dataset splits are given in [Table 2](#). For Dataset-G, we performed the augmentation to balance the sample distribution per age range ([Fig. 2](#)).

As the shoeprint images in our dataset are not perfect and complete as found in ideal scenarios. The shoeprint images in the given dataset can be found in scratched, abrasive, noisy, partial, and so on, which match with images obtain in forensic scenes. Moreover,

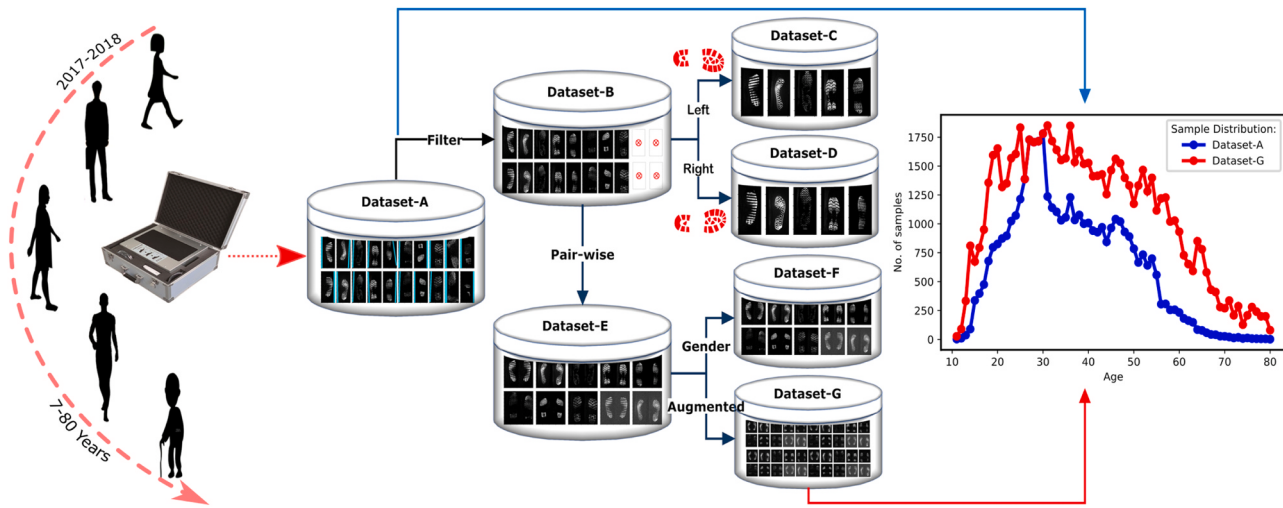


Fig. 2. The overall generation of datasets generation and sample distributions, with brief descriptions, as which appear in Table 1. There are seven versions of shoeprints datasets including: Dataset-A, unprocessed and original shoeprints; Dataset-B, wherein the scale/ruler and poor-quality images are discarded manually; Dataset-C, which contains only left shoeprints; Dataset-D, which has only right shoeprints; Dataset-E, which is comprised of the horizontal concatenated left and right shoeprints into a single pair-wise shoeprint; Dataset-F, generated for gender-based classification and age estimation, and Dataset-G, the augmented dataset used to balance sample distribution in group-wise age prediction. The distributions of two datasets (Dataset-A and Dataset-G) are visualized. (For interpretation of the references to color in this figure legend, the reader is referred to the web version of this article.)

extensive amount of data collection is a challenging task while the deep learning models need huge amount of information to learn knowledge. So, a model trained our dataset can be utilized for realistic scenarios.

2.2. Segmentation and superimposition

The acquired shoeprints were processed for studying group-wise pressure distributions. For each group, the images were superimposed to analyze the pressure distributions. First, a threshold value was set up after converting the color images to gray-scale images using Open CV [55]. In image processing, superimposition generally refers to the placement of one image on top of existing image(s) to reflect the overall effects [56–58]. To find the bounding box of shoeprints as a stage of superimposition, the images were processed for finding contours. The corresponding bounding boxes were computed for each contour, pruned down contours by figuring out the minimum top-left and maximum bottom-right coordinates. For superimposition in our case, we first segment shoeprint from a complete image precisely by avoiding both the edge-cutting and inclusion of extra regions. We made sure the segmentation of shoeprint from a complete image is precisely extracted by avoiding both the edge cutting and inclusion of extra regions. The segmented regions are variant in terms of the bounding-box size caused by dimensional variations in shoeprint images. For instance, the subjects from one age group (e.g., 21–30) may have shoeprint images taken in different sizes, which need to be standardized in both width and length (a requirement of most machine learning models). We then crop the images based on the bounding-box coordinates and

resize them into the same aspect-ratio by the inter-cubic interpolation to circumvent moire patterns [59]. The segmented images are then flipped to the same natural bearing direction as left and right shoeprints. All the segmented images are then stacked with same coordinates for each age group (e.g., 21–30, 31–40, etc.). To find the pressure variations from preceding to next group, we converted all images to the integer-16 (i.e., -32,768 to +32,767) datatype to keep both negative and positive results. Both positive and negative range of values enable superimposition to keep the absolute subtracted pixel-values reflecting pressure distributions. We randomly sampled from each age group and made sure the precise segmentation and alignment processes. The main purpose of superimposition of shoeprint images is to investigate the force trends in each region of the images having the same boundary size corresponding to individual age groups.

2.3. Evaluation metrics

For a regression problem of age prediction, we apply cumulative score (CS) and mean cumulative score (MCS) as evaluation metrics to accommodate the nature of the problem. CS and MCS imitate the existing studies [60–62], and are used to assess accuracies in a range of age groups. CS (or CS_j) and MCS (or MCS_j) give more weight to the smaller ranges of match windows. The ranges depend on the value of j and J , the absolute differences between actual and estimated age scores, as shown in the following:

$$MCS - J = \frac{\sum_{j=0}^J CS_j}{J + 1} \quad (1)$$

Table 2

Data distribution of males and females in the original and augmented datasets.

S.No	Dataset		Augmented		Total		Grand Total
	Male	Female	Male	Female	Male	Female	Male+Female
Original	24,371	5120	—	—	—	—	29,491
Training	22,871	3620	—	21,100	22,871	24,720	47,591
Validation	—	—	—	—	—	—	10% of 47,591
Testing	1500	1500	—	—	—	—	3000 of 29,491

Male subjects have much more samples than female subjects. To address the imbalance, the female samples were augmented from 5120 to 22,871. So, a total of 47,591 samples were used for training, in which 10% were used for validation, and 3000 of the original samples were used for testing.

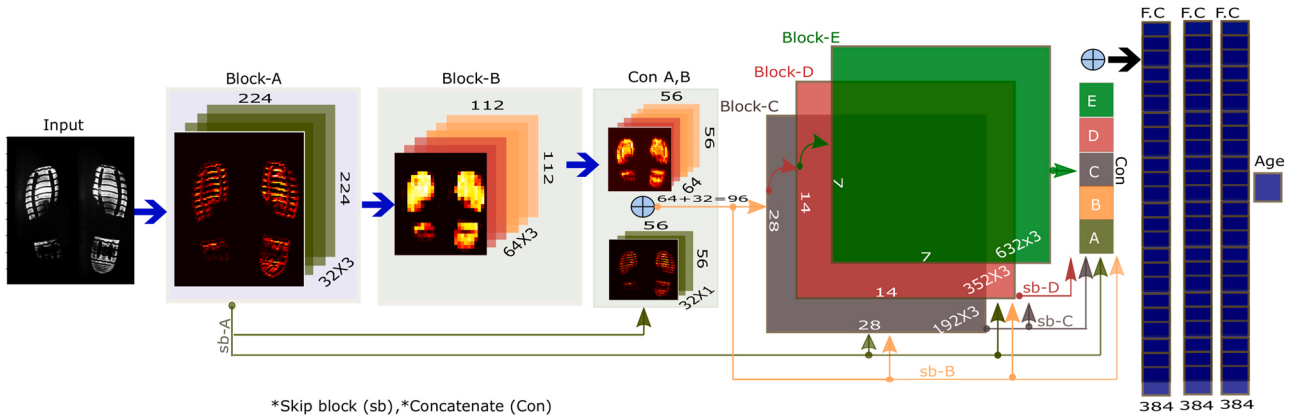


Fig. 3. Architecture of the proposed model (ShoeNet). Each input image of shoeprints is 224 by 224 pixels. There are five blocks (Blocks A, B, E). The output of each block feeds as the input to the next block, i.e. Block-A to Block-B, and Block-B to Block-C, and so on. The internal block structure contains a stack of convolution operations; in particular, Block-A has 3 feature maps of 32 filters, and the dimension reduces by 2 fold across each block (down-sampling). Each block outputs down-samples, skips to the next block (sb) and merges (i.e. Con A,B) together to produce the input for the deep level block. The skip connections are shown with arrows, while all the blocks merge in the last layer shown with the \oplus operation. After skipping and merging, there are 32 and 64 feature maps for Block-A and Block-B, respectively. While after the concatenation, the number of feature maps increases to 96. Finally, all the fully connected (FC) layers end up with a single neuron for age prediction.

$$CS_j = \frac{\sum_{i=1}^n \delta_i}{n} * 100$$

where

$$\delta_i = \begin{cases} 1, & \text{if } \delta_i \leq j \\ 0, & \text{if } \delta_i > j \end{cases}$$

CS_j is the percentage mean of δ_i , where δ_i is the Euclidean-distance ($|y_i - \bar{y}_i|$) between actual (y_i) and predicted (\bar{y}_i) score, and it will be counted as 1 for $|y_i - \bar{y}_i| \leq j$. The value of δ_i expressed as zero (0) implies that the distance ($|y_i - \bar{y}_i|$) is greater than the threshold value (j). The MCS score facilitates prediction in various ranges of matching thresholds rather than a single threshold. Thus MCS score gives a more comprehensive assessment for the challenging problem of shoeprint-based age prediction to cover all the values of $|y_i - \bar{y}_i| \leq j$ for the setup threshold (j). This also allows us to give different penalties with varying thresholds in the objective function of the deep learning model.

2.4. Regression specific custom loss function (CLF)

Because age prediction is a regression problem, a single output will be expected as a result. For empirical significance, we customize the mean-square-error (MSE) into a specialized form (CLF) to optimize the hyperparameters during training. The optimizer (Adam) fine-tunes the weights of convolution filters to minimize the loss value. To produce regression specific results, CLF penalizes the out-ranged values more. It minimizes the distance between the actual and predicted age in a target-oriented way. The formulation of CLF is illustrated in the following equation:

$$CLF = \frac{\sum_{i=1}^n E_i}{n}; E_i = \begin{cases} d_i * \epsilon, & \text{if } d_i \leq J \\ d_i^3 + \epsilon, & \text{if } d_i > J \end{cases} \quad (2)$$

CLF is the mean of difference (E) for n number of samples, where $n = (\text{total-samples}) / (\text{input-size})$. ϵ is a small value (0.0001-to-0.3) used to prevent the network from attaining zero difference and to sustain the learning process. Similarly, $d_i = |y - \bar{y}|$ is an absolute error between actual-age (y) and predicted age (\bar{y}). Furthermore, J is a natural number derived from MCS-J for predictable age ranges. In the second condition ($d_i > J$), the values higher than the value of J will cause more penalization of the weights based on the computed loss-value in the exponential time (power 3). The penalization influences the optimization of network weights and biases. It will direct the

optimizer to tune these parameters in order to minimize the difference between actual and predicted age. The CLF values for $J=2$, $J=3$ and mean-square-error (MSE) are illustrated in [Supplementary Fig. S2](#). The CLF values indicate abrupt changes for $J=2$ and $J=3$, which demonstrates a high penalty by following that the MCS-J would be only counted in the given range of J . To verify the effectiveness of CLF, we carried out the training of our proposed model (ShoeNet) based on both CLF and a mean-square-error (MSE) loss function up to 500 epochs. In which, MSE finds the mean square difference of actual and predicted values and, therefore, gives more significant value to MAE rather than MCS-J ($J = 2, 3, \dots, n$). On the other hand, CLF not only considers the absolute error as well as penalizes more the adjacent values to J in MCS-J. By directing for more penalization, the given optimizer fine tunes the learning weights to obtain a persuasive estimation score. Adam is used as an optimizer with the L-2 regularizer to tune hyper-parameters.

2.5. Prediction models

2.5.1. ShoeNet architecture for age prediction

ShoeNet is designed to effectively learn the wear-effects on shoeprints varying with gait and standing patterns corresponding to age progression. It is based on pairwise shoeprints and captures extracted features from left and right shoeprints. The features learning by deep models is considered as black-box which cannot be unfold to human. As a unified pair-wise shoeprints representation, ShoeNet extracts feature maps in order to obtain the wear effects reflecting the walking characteristics of individuals. ShoeNet is equipped with a skip mechanism to re-parameterize the stack of features at the next convolutional layer. ShoeNet utilizes a customized loss function in a target-oriented fashion to handle the outliers in the data. The architecture of ShoeNet is shown in [Fig. 3](#). ShoeNet adapts the concept of skip-connections from Residual-Net [\[63\]](#) and a dense structure from DenseNet [\[64\]](#). The skip layers integrate the learned features from early levels, which help them avoid the degradation of shallow stacked networks and circumvent the gradient information loss to maintain features of gait and standing patterns in the corresponding pair-wise shoeprints ([Supplementary Fig. S3](#)). The parameter sharing in the form of skip-block enables the model to learn holistic age-related features from shoeprints.

ShoeNet is the integration of five convolution blocks (Blocks-A, B, C, D, E), three fully connected layers and a single output of linear regression for age prediction ([Fig. 3](#)). All the stacked convolution layers inside the blocks are followed by pooling,

batch-normalization (BN), and rectified linear units (ReLus). At the higher level, the fed images are passed through BN and ReLu functions prior to convolution layers. Each block is connected to the next block in two ways: first, the output of the earlier block feeds as the input to the next deep level block, for instance, Block-A inputs to Block-B, Block-B inputs to Block-C, and so on. Second, the output of each block, except for the last layer, skips and down-samples to all the deep block as skip-layers and merges with the corresponding block. For instance, block-A skips and down-samples to the corresponding dimensions of deeper blocks (i.e., Block-C, Block-D, and so on) and merges along the specified axis with the output of Block-B, Block-C, and so on. Finally, all the skipped and convolutional layers merge channel-wise into a stack of representations and then densely connect with three fully connected layers leading to a single output as age prediction. The three fully connected layers contain 384 neurons each, with a single neuron for the last layer.

In order to convolve the feature-maps speedily and converge the weights and biases for achieving the target, we converted the color images into grayscale number of channel as one(1). After resizing, the dimensions of each image are height $H(224)$, width $W(224)$ pixels and the number of channels $N(1)$. During ShoeNet training, the images feed as the integration of (Input_size, 224, 224, 1). At the higher level, by applying the BN function followed by ReLu, the training process accelerates, and brings smoothness and regularization in the loss function landscape as well as reducing the covariate shift. The three stacked shallow convolution layers are structured as (X_i, F_n, F_s) , where X_i is the input from the previous layer, F_n is the number of filters, and F_s is the filter-size. For instance, the parameter arrangement for Block-A is $(224 \times 224, 32, 3 \times 3)$, representing the input dimensions, number of filters and filter window-size, respectively. Similarly, for Block-B $(112 \times 112, 64, 3 \times 3)$, the input dimensions were down-sampled while doubling the filter size, and so on. The skip layers cumulate after merging with the next layer followed by BN and ReLu. Merging at Block-E produces $A \oplus B \oplus \dots \oplus E$, where \oplus corresponds to the concatenation operation (Fig. 3). For matching the number of feature maps, each skip layer down-samples and up-samples after applying 1×1 convolution to maintain learned features at a higher level and avoid significant performance degradation (Supplementary Fig. S3). To avoid overfitting, the fully connected layers drop out by 30%, 40% and 50% rate, respectively.

Before training the model, 18,111 poor-quality images were removed. Among the remaining 81,889 images, 40,000 images were

used for testing, 10% of the other 41,889 images for validation, and the rest were used for training up to 100 epochs. Moreover, the L-2 regularizer with a weight decay of 0.001 embeds in the second-last fully connected-layer to avoid large weights by pushing the weights toward zero (0). The Adam optimizer tunes the networks weights from the initial learning rate (LR) 0.001, $\beta_1(0.99)$, $\beta_2(0.999)$, epsilon (1e-08) and learning-decay-step 10,000 based on the loss value of CLF.

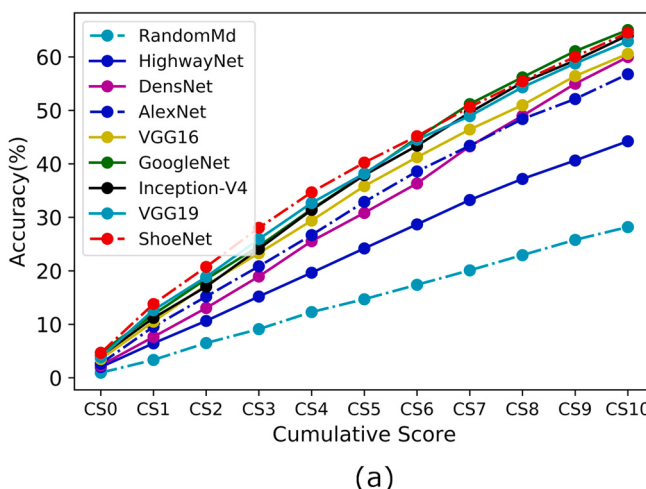
2.5.2. ShoeNet for gender classification

We examined patterns of pressure spreading on shoeprints that varied from males to females. First, we classify the gender by deploying a two-class based prediction. For gender classification and gender-based age analysis, we trained and validated ShoeNet structure with balanced dataset-F (Table 2). The left and right shoeprint images in dataset-F are separated for both male and female and combined pairwise as wear by human in natural way. This would enable the model to learn asymmetric features from pair (i.e., left and right) of shoeprints vary from male to female. As a classification problem, the same ShoeNet structure (Fig. 3) was modified with minor changes in terms of the number of neurons in fully connected layers. After modification, the number of neurons were 512, 384 and 256 for the corresponding three fully connected layers, while the last layer had a two-neurons output with a softmax activation function to perform classification. We applied categorical cross entropy as the loss-function, with Adam optimizer, and Accuracy and Confusion as evaluation metrics.

3. Results

3.1. ShoeNet vs. state-of-the-art models

We compared the ShoeNet architecture with some state-of-the-art (SOTA) deep learning based models. The models for the comparative study against ShoeNet included Random-Method (RandomMd), HighwayNet [65], DenseNet [64], AlexNet [66], VGG16 [15], GoogleNet [67], Inception-V4 [68], and VGG19 [15]. All the underlying models were trained using similar objective function (L2), optimizer (Adam), number of samples, sample dimensions, and so on. To compare against a baseline, we used RandomMd, which is based on the random numbers generated to validate by-chance age prediction. All the models were trained and tested for age estimation with the same dataset and similar hyper-parameters. For



(a)

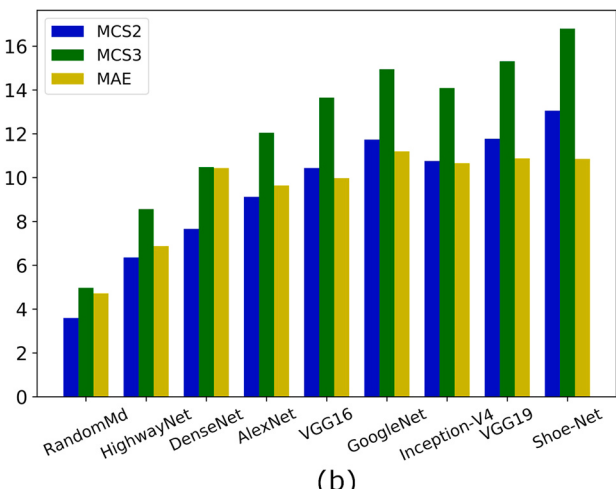


Fig. 4. Comparison between ShoeNet and other SOTA deep learning models. (a) The cumulative scores of ShoeNet and standard models are depicted in terms of CS_j (for $j = 0, 1, \dots, 10$). ShoeNet has a similar trend with GoogleNet in terms of CS_j (for $j > 6$) but ShoeNet has a higher score of CS_j (for $j \leq 6$) than any other model within the prediction range. (b) The bar graph is the depiction of three evaluation parameters with standard modalities, including MAE percent-accuracy, MCS-2 and MCS-3. The detailed statistical results are listed in Supplementary Table S1. (For interpretation of the references to color in this figure legend, the reader is referred to the web version of this article.)

performance assessment, cumulative score (CS), mean cumulative score (MCS) and mean absolute error (MAE) percent accuracy were applied (see Methods), and the comparative illustrations are shown in Fig. 4. CS_j can be computed as the counting of all those subjects whose age differences (between ground-age and predicted-age) are within the given range ($j = 0, 1, 2, \dots, 10$), and then divided by the total number of test samples (n) and multiplied by 100. For instance, the true predicted score (CS_2) for a given range ($j \leq 2$), will be the sum of all subjects whose age differences are within 2 years and divided by n , and then multiplied by 100. Similarly, $MCS-J$ computes the mean of $CS_0, CS_1, CS_2, \dots, CS_J$ scores. In contrast to a single assessment value for regression, these metrics evaluate the prediction performance in a broad relevant range. Using these metrics, ShoeNet reported higher scores of $MCS-2$ (13.06) and $MCS-3$ (16.81) than other methods. ShoeNet also presented an acceptable percent accuracy score (Fig. 4(b)). The prediction accuracy of a subject to the ground-truth range is about 40% if taking the 5-year threshold (i.e., $J = 5$, see Fig. 4(a)) and about 81% if taking 15-year (i.e., $J = 15$, see Fig. 4(a)). The overall prediction scores CS_j ($j = 0, 1, 2, \dots, 10$) of ShoeNet and SOTA models are shown in Fig. 4(a).

In addition to the comparison against the SOTA models, we also trained ShoeNet with both CLF and MSE objective functions to highlight the performance of ShoeNet by inclusion of CLF (Table 3). The evaluation metrics ($MCS-2, MCS-3$) are remarkably superior for ShoeNet trained with CLF. In particular, CLF-based ShoeNet has higher evaluation scores than MSE-based trained network. The customization of CLF leads to a faster and better convergence rate toward actual age.

3.2. Deep learning approaches for shoeprints based biological traits analysis

It is expected that pair-wise shoeprints have more age-related information in standing and gait-patterns than in an isolated single shoeprint. To better utilize the information for age prediction, a number of dataset versions were formed (Table 1), and several deep learning models were developed corresponding to the nature of the datasets (Fig. 2). The detailed descriptions of training, validation, and testing of these datasets and their modalities are placed in Supplementary Method. Our deep models consist of a Left & Right shoeprint based convolution neural network (LR-CNN) (Fig. 3), a fusion model (FM-CNN) (Supplementary Fig. S4) and a multi-model architecture (MM-CNN) (Supplementary Fig. S5). The datasets used for training LR-CNN, FM-CNN and MM-CNN are both Dataset-C and Dataset-D, while ShoeNet was trained on Dataset-G (Table 1). LR-CNN extracts features from a single shoeprint (either left or right). FM-CNN combines dissimilar features extracted by a twin network corresponding to the two shoeprints (L&R). Furthermore, MM-CNN incorporates parameter sharing and an ensemble approach to map the shoeprint features with human age. It contains multiple architectures and allows each architecture to benefit from isolated features. All three modalities capture complementary features. In contrast to LR-CNN, FM-CNN and MM-CNN, ShoeNet interprets both

Table 3

Comparative evaluation-scores of ShoeNet trained with Custom-Loss-Function (CLF) and with MSE loss functions.

Network	%MAE	CS_0	CS_1	CS_2	CS_3	$MCS-2$	$MCS-3$
CLF	11.20	4.3	13.14	20.69	27.09	12.71	16.305
MSE	11.07	4.04	12.84	19.49	25.73	12.12	15.52

CLF was customized for ShoeNet to predict age, in which the loss values out of the range are treated with more penalization than the in-range values. The percent accuracy of CLF-based ShoeNet is less accurate than the MSE-based trained ShoeNet. Similarly, the cumulative scores including $MCS-J$ ($j = 2, 3$) are also significant for ShoeNet model trained with the CLF loss function. CLF ($j = 2, 3$) and MSE based loss values are visualized in Supplementary Fig. 2.

Table 4

Four main network modalities and their corresponding values for MAE, $MCS-2$ and $MCS-3$.

Networks	Network-Types	MAE	$MCS-2$	$MCS-3$
LR-CNN	a -Left-Shoeprints	9.38	11.52	15.16
	b -Right-Shoeprints	9.70	12.12	15.70
	c -Left-to-Right Shoeprints	9.51	10.49	13.78
FM-CNN	a -Early-Fusion	9.48	10.19	13.60
	b -In-Fusion	9.78	11.19	14.74
	c -Late-Fusion	9.45	9.91	13.15
MM-CNN	a -Early-Sharing	8.99	11.09	14.59
	b -Middle-Sharing	9.10	10.74	14.31
	c -Late-Sharing	9.72	9.96	13.35
ShoeNet		9.21	13.06	16.80

The four main network modalities are customized using the generated datasets for training. Each modality uses left and right shoeprints for training while having a distinct way of processing. The four modalities are further divided into sub-networks having distinct internal structures. In the first category, the right shoeprints-based network has a higher score. Similarly, in the fusion modalities of FM-CNN, In-fusion has a significantly better result than early and late fusions. Furthermore, the early sharing model has a significantly better result than middle or late sharing. Overall, ShoeNet has the highest cumulative score and outperforms the other modalities, although the mean absolute value is not significant for ShoeNet as a result of customization in the loss function leveraging evaluation metrics ($MCS-j$).

(L&R) a single representation to estimate the age. It takes both shoeprints as a single input image to utilize the representation of gait patterns in the corresponding opposite shoeprint as illustrated in Supplementary Fig. S3. ShoeNet outperforms all the other models with $MCS-2$ (13.06) and $MCS-3$ (16.80) while producing an acceptable result for MAE-percent-accuracy (Table 4).

3.3. Result analysis of group-wise aging

We analyzed the significance of ShoeNet in terms of group-wise aging and consistent variations of pressure effects on shoeprints caused by gait and standing patterns. To better depict the aging association with shoeprints, we categorized shoeprints into two types, i.e. Type-A and Type-B. Type-A is divided into three sub-categories in terms of age groups, which are 10–80 (ShoeNet main-category), 20–50 and 25–45 year olds, while Type-B is sub-divided into cat-A (10–20), cat-B (21–30), cat-C (31–40), cat-D (41–50) and cat-E (50–80) year olds, as shown in Table 5. In addition, ShoeNet associates the relevant wear-effects with respect to the group-wise age estimation. As shown in Table 5, Type-A has the best performance in the category of 25–45 year old subjects. Similarly, in Type-B, cat-B (21–30) has highest scores in $MCS-2$ (17.86) and $MCS-3$ (22.67), which indicates that the subjects in cat-B (21–30) have more consistent effects of gait and standing-patterns on shoeprints than other age groups. Furthermore, the performance in cat-E (51–80) is relatively poor given the inconsistent gait-and-standing patterns

Table 5

Statistical results for age estimation in different age groups.

Age Ranges in Years	MAE Mean Absolute Error	$MCS-2$	$MCS-3$
Type-A	9.21	13.06	16.80
	7.51	15.16	19.55
	6.44	17.59	22.00
Type-B	10.80	9.24	11.12
	6.77	17.86	22.67
	6.23	16.52	21.38
	10.05	9.64	12.87
	18.82	2.4	3.4

Type-A has three subtypes while type-B has 5 subtypes based on the age ranges. Type-A has the best MAE (6.44) and $MCS-J$ (17.59 for $J = 2$) scores in the age group ranging from 25 to 45 years old. Similarly, Type-B has the best score of MAE (6.23) for the age group of 31–40 years old while category 21–30 has the best $MCS-J$ score (17.86 for $J = 2$).

and pressure distributions on the shoeprints. The elder subjects above 50 years have diversities in their health conditions. For instance, some people might have advanced age but healthy conditions, which may show youthful walking and gait patterns, while some other people may have severe diseases that affect walking and standing.

3.4. Trend analysis of group-wise pressure distributions with aging

To investigate the pressure distribution on shoeprints in standing and walking, an age group-based study can reveal the association of gait and standing-patterns with age. Furthermore, the examination of pressure distributions on each region of shoeprint validates a suspect's identity to particular age group and sex. After age prediction and gender classification, further evidence, identification, and confirmation of a suspect demographic (age, gender, race, ethnicity, etc.,). For this purpose, we used the division of Type-B in five categories (cat-A, cat-B, cat-C, cat-D, and cat-E) as mentioned above and shown in [Table 5](#). All the shoeprints in each category were superimposed after segmentation and averaged along the given axis (see Methods). After the superimposition, L&R shoeprints were obtained for each category. To depict the pressure trends, the corresponding subtraction process was performed for each category, i.e., the lower category subtracts from the higher category (e.g., cat-B-cat-A) along the given dimension, and this process continues for each category from that point on (see Methods). It can be deduced that the pressure distribution changes reflect pattern variations from one group to the next older group caused by aging, as shown in [Fig. 5](#). The highlighted regions show that the front foot pressure is mainly on the first toe (hallux) as indicated in the first row of the [Fig. 5](#), but it spreads toward other toes as shown in both the first and second rows. This pattern is also true for other areas, as the changes from (cat-B-cat-A) to (cat-E-cat-D) indicate that the high-pressure distributions shift to the outward regions of the heel with age progression. In particular, the first subtracted category (cat-B-cat-A) shows this category shift as the most distinctive, indicating obvious changes in pressure trends between the subjects of cat-A and cat-B. In the second superimposed subtraction (cat-C-cat-B), these pressures continue to shift toward the exterior regions of shoeprints but

to a much lesser extent. Similarly, these pressures further move to the most exterior parts of shoeprints (cat-D-cat-C), with a slightly more pronounced shift toward the heel of the right shoeprints-moreso than toward the left shoeprints. Finally, the pressure shifts to the front toe area from cat-E to cat-D. These visualizations illustrate that the muscle forces reflected in shoeprints have a clear trend of variations from younger to elder ages.

To further extrapolate the pressure distributions on shoeprints, the superimposed L&R images of each category are divided into eight regions ($R_0, R_1, R_2 \dots R_7$) ([Fig. 6\(a\)](#)), and each region is depicted in curve trends as illustrated in [Fig. 6\(b\)](#). These regions separately show the pressure trend variations with respect to age. The similar pressure distributions are portrayed when the upper and lower boundaries of shoes are aligned without the overall shown superimposition ([Supplementary Fig. 6](#)). While in most areas, the patterns are symmetric between the left and right shoeprints, some clear symmetries are also observed. In the regions R_0, R_1, R_3, R_4, R_7 , the intensities or pressure regions on both L&R shoeprints spread increasingly from the early-age group (cat-A) to the middle-age group (cat-C) and then slightly decline trends in the elder-age group (cat-E) as shown in ([Fig. 6\(a\)](#) and (b)). Noticeably, region R_2 of both L&R shoeprints has the most robust increasing trends of pressure over aging. A similar trend can also be noticed in Region R_7 of the right shoeprints but are not quite as noticeable in left shoeprints. The overall observation is that the pressure increases up to 40 years and steadily maintains on the outer part of the shoeprints ([Fig. 6\(a, b\)](#)). The pressure intensities decline clearly after 40 years of age in regions R_0, R_1, R_3 and R_5 but to a less extent in R_2, R_4, R_6 and R_7 . Overall, such a pressure decrease with aging in the inward regions is more pronounced than in the outward regions. The same pressure spread can also be seen in category-wise subtraction from the early-to-late ages ([Fig. 5](#)), while the subtractions of cat-A from the rest of the categories (cat-B, cat-C, cat-D, cat-E) are also visualized in [Supplementary Fig. S7](#). With aging, the most visible changes are detected in the heel regions (R_6, R_7). Moreover, on left shoeprints, the pressure on region R_2 reaches or even exceeds R_1 . All the pressure trends are cumulatively plotted for the corresponding left and right shoeprints along the age ranges (along the x-axis) as shown in [Fig. 6\(c, d\)](#). The cumulative plotting comparatively represents the

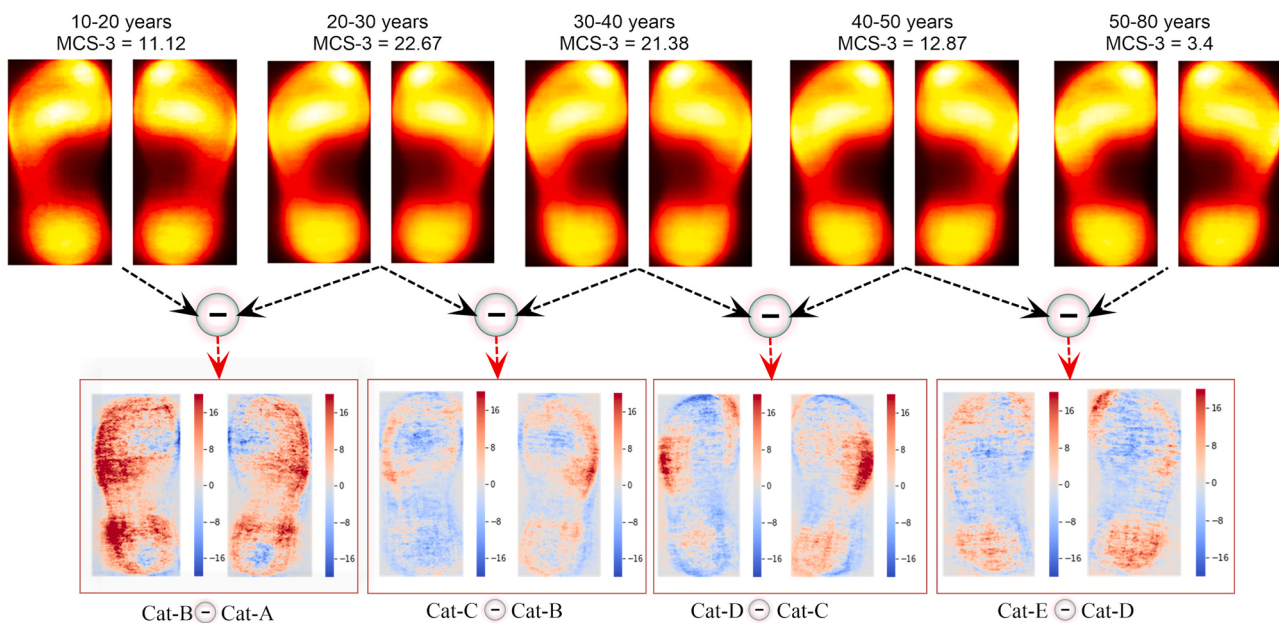


Fig. 5. Category-wise pressure distributions on shoeprints with respect to age. The five age categories are shown with their corresponding MCS-3 values in the age prediction. The first row depicts the pressure distributions of the five-categories based on the given age ranges. All the visualized images are the average of superimposed shoeprints in each category. The second row renders the subtracted pressure differences between two neighboring categories.

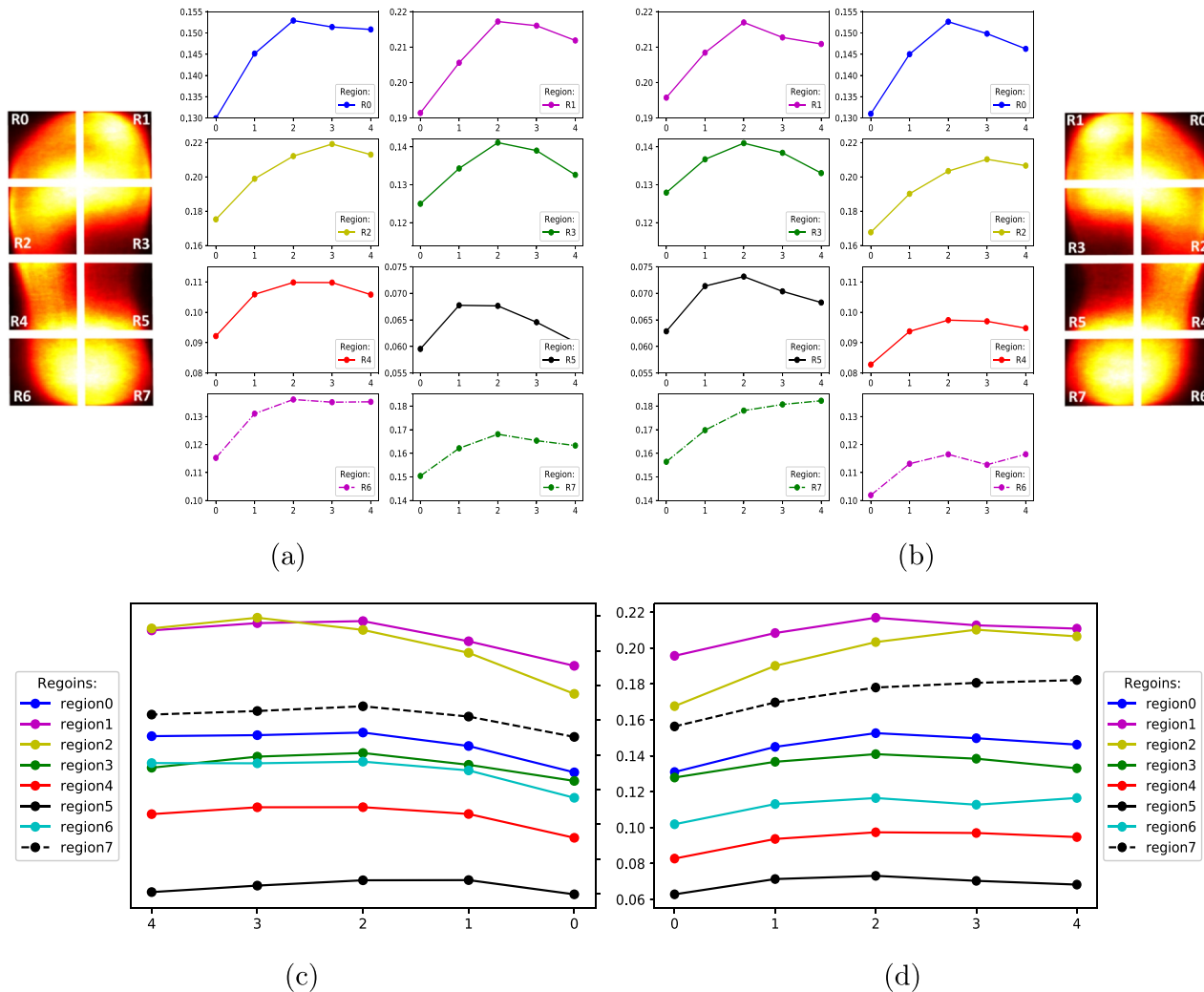


Fig. 6. The category-wise pressure distributions on shoeprints with respect to age for the 8-regions of L&R shoeprints. In the first row, the left most and right most shoeprints are sampled from the average of superimposed shoeprints to visualize the divided eight regions. All the plots are demonstrated with pressure intensity values along the y-axis and aging along the x-axis. There are five age-based categorical division along the x-axis, with each group comprised of subjects according to their ages. For instance, Group 0 (Cat-A), Group 1 (Cat-B), Group 2 (Cat-C), Group 3 (Cat-C), Group 4 (Cat-D) and Group 5 (Cat-E) along the x-axis represent ages ranging of 7–20, 21–30, 31–40, 41–50 and 51–80 years, respectively. All the shoeprints in their corresponding category are superimposed and then averaged to demonstrate the pressure trends. (a) and (b) show the category-wise aging effects in pressure distributions over eight divided regions in the given age ranges for left and right shoeprints, respectively. (For interpretation of the references to color in this figure legend, the reader is referred to the web version of this article.)

evaluation of categorical age-ranges, which reveals variational effects in distinct periods of age groups.

3.5. Shoeprints vs. gender

3.5.1. Gender classification

We analyzed the trends of pressure distribution changes for group-wise age groups based on gender. To substantiate the gender-based patterns, we proposed a gender classification network from shoeprints based on ShoeNet, which trains on Dataset-F (see Methods). After training, we observed noticeable results with 89.34% training and 86.07% testing accuracy for gender prediction. The evidence in the corresponding confusion metric demonstrates the significant classification results (Table 6). The classifier predicts gender with a high accuracy (86.07%), which infers obvious differences in patterns between males (M) and females (F) in pressure distribution.

Table 6
Gender-based classification report with significant (86.07%) accuracy.

	Precision	Recall	F1-score
Male	0.8360	0.8973	0.8656
Female	0.8892	0.8240	0.8554
Testing accuracy	86.07%		

3.5.2. Pressure distributions between male and female

Males and females are found to vary in their gait patterns as they grow older. These variations can be seen for males and females in Fig. 7, which shows males to have more pressure distribution toward the instep area than females. In females, the pressure varies significantly below 20 and above 40 years old. Similarly, male subjects show more pressure trends from early age to the age of 30 years; then, the pressure tends to flow smoothly toward shoeprint edges. In most cases, for both males and females, the right shoeprints are observed to endure more pressure forces with age.

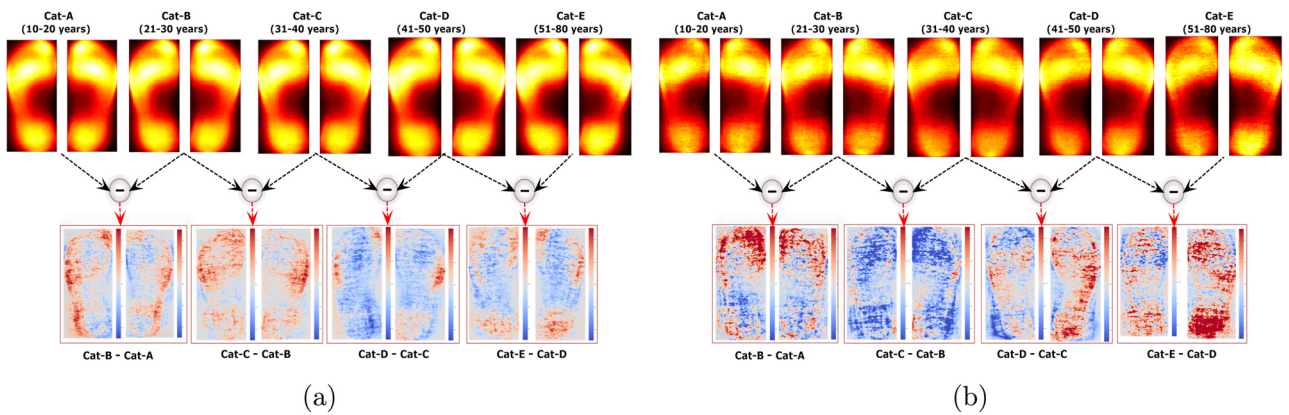


Fig. 7. The first row shows the superimposed shoeprints of five categories (category-A, B, C, D, E) for age ranges 10–20, 21–30, 31–40, 41–50, and 51–80 years, respectively. The second row depicts the lower category subtraction from the upper category; for instance, Category-B minus Category-A. The shoeprint pressure distribution versus age in (a) males and (b) females, respectively.

3.5.3. Region-wise pressure distribution between male and female

Similarly, the average (superimposed) image of every age group is divided into eight regions in the same manner as shown in Fig. 6, which is visualized from early age (cat-A) to late age (cat-E) as shown in Fig. 8, based on male-female-left (MFL) and male-female-right (MFR) pressure related images. A large variable to aging is observed in the back-foot/heel region representing R_6 for females while the males do not have such a pattern. Region R_2 of MFL and MFR has some similar variations in the pressure range between 57.5 and 70.0 per unit area. Regions R_2 , R_4 and R_5 of the corresponding MFL and MFR have similar patterns in pressure trends relative to aging. However, regions R_4 of both MFL and MFR, and R_7 of MFL have some opposite pressure trends with aging in both males and females. The overall analysis shows that males (red) have higher pressure trends than females (green) except in regions R_0 of both the left and right shoeprints, indicating a higher force used by females in this region, which is interesting. Collectively, we have a total of four sets of curves, each for male-left shoeprint (ML), female-left shoeprint (FL) (Fig. 8(c)) as well as for the male-right shoeprint (MR) and female-right shoeprint (FR) (Fig. 8(d)). From the depictions, we can observe that for region R5, lower pressures are common in ML and FL shoeprints. Furthermore, MR and FR shoeprints in regions R1 and R2 have higher pressures. Shoeprint regions R_0 , R_3 , R_4 , R_6 and R_7 in ML have uniform variations in pressure trends while R_0 , R_3 and R_4 of FL have similar distributions. In most cases, the pressure is higher for the male interior parts of L&R shoeprints while females are only found to have higher pressure in the front toe (R_0). In conclusion, males and females have fluctuations in pressure forces in the form of shoeprints generated by gait and standing patterns with respect to age growth. Such fluctuations in pressure trends can be reasoned by body weight between males and females which are also reflected in terms of pressure distribution.

3. Discussion and conclusion

The main objective of this study is to estimate human age and gender from imprinted shoeprints via a machine-learning approach. Shoeprints are influenced by the human gait and standing patterns, which are further attributed to aging. This is reflected in the shoeprint patterns for subjects under different age groups in different genders. We also demonstrated that ShoeNet can utilize such patterns to predict the human age and gender effectively. This study helps to extend the frontiers of shoeprint applications from forensic investigations to diverse areas including biological profile estimations, examining health and sports activities, and clinical investigations. For example, in some cases, estimated physiological

(biological) and actual (chronological) ages may not match well under different health conditions. For instance, some people look younger or older than their chronological age. Physiological aging could slow-down with a healthy environment, lifestyle, physical and cognitive functions [69]. Predicted physiological age of an individual versus his or her actual age may provide some insight into the health conditions.

The prediction is based on the relationships among physiological aging, walking and gait patterns, and imprinted shoeprints (see Fig. 1). The variational effects are associated with the body muscles which are reflected by the forces during walking and standing on the ground surface in the form of foot impressions/shoeprints. The natural wear-and-tear appearance shown in the shoeprints can be used to predict age by involving distinct contact regions of the footwear. The crime scene investigation process composed of many stages, start from planning and evidences collection to preservation and clinical forensic. Our proposed study aids the clinical investigation from the collected evidence (shoeprints) to narrow down a large scale of population to a small number of suspects. As such, the forensic investigation team may use the highly reliable recognized profile of the subjects who left the shoeprint(s) together with other biological traits (i.e., DAN, fingerprint, etc.) to identify the suspect from a much smaller pool of potential suspects. Thus, our machine learning model is capable of saving much time and resources of the investigators by filtering the suspects by sex (e.g., male or female) and age (e.g., 21–30).

Age estimation is a challenging task even from facial, brain MRI [33,34], EEG [35] and DNA [36] due to many intrinsic and extrinsic factors including genetics, diet, hormones, and lifestyles. Technical challenges include insufficient labeled data and advanced computational methods. This study addresses both challenges by providing large-scale labeled data and a machine learning approach. It provides a benchmark for shoeprint-based age estimation by the availability of large-scale datasets and dataset-specific models. Our machine-learning model successfully addresses computational issues related to data noises, variational patterns, manufacturing designs, wear-time, and most importantly wear effects [4,17]. In this study, the machine (deep) learning approaches are accomplished for age prediction within 5-years age ranges (CS₅). We had a good CS₅ score of 40.23%, and we also scored 86% accuracy in classifying shoeprints in term of gender classification. It shows that the deep learning model learns knowledge from a large given dataset and extracts end-to-end features for aging and gender. The model is capable of capturing aging effects, which can be further improved by including more label information such as gender, height and weight.

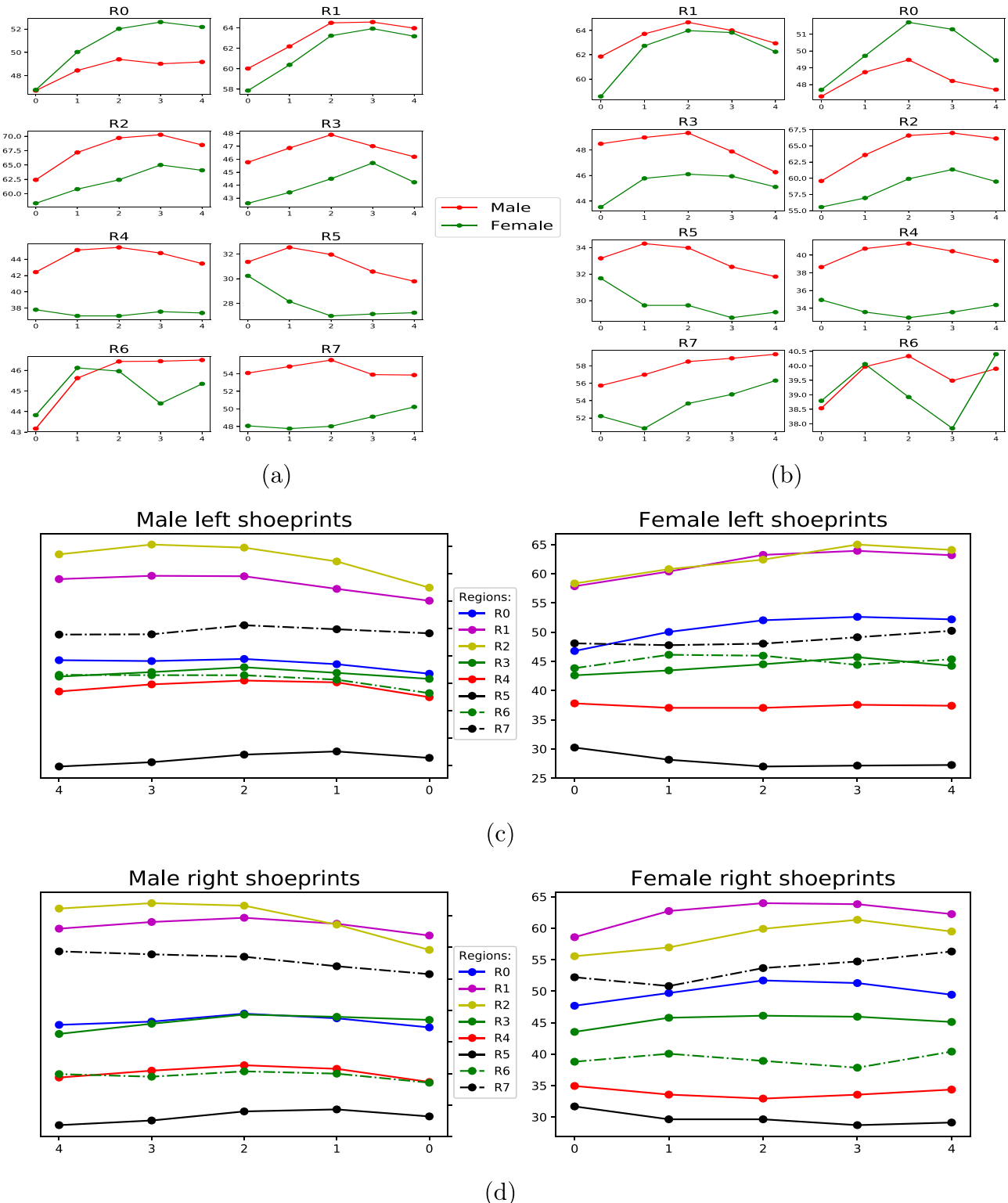


Fig. 8. Category-wise aging effects in pressure distributions over eight divided regions between males and females, derived from the superimposed L&R shoeprints of male-and-female (M&F) in the given age ranges from cat-A to cat-E. Fig. 6(a) and (b) show a similar scale for pressure intensities along the y-axis and for age groups along the x-axis, which cover the eight regions for M&F for (a) left shoeprints and (b) right shoeprints. Each region has two curves. The red curve represents males, and green represents females. Collective trends are shown in (c) with male left shoeprints and female left shoeprints, and (d) with male right shoeprints and female right shoeprints. The relative regions with the same scale are shown in Supplementary Fig. S8. (For interpretation of the references to color in this figure legend, the reader is referred to the web version of this article.)

This study collected shoeprints from 50,000 subjects with annotations of age and gender, which derived a variety of datasets. To train a reliable deep model, it is critical to feed the data with insightful features and to achieve at least the average performance. The data need proper preparations and pre-processing includes

addition, deletion, or transformation prior to training a machine learning model. Thus, we have discarded the poor quality images. However, the inclusion of poor quality and less perfect images should be part of the training samples to adhere the forensic circumstances. Although our model is designed to be deployed for

forensic circumstances, we trained the model using clean (high quality) data to reduce the effects of noises, which is a limitation on the requirement of high data quality widely observed in nearly all deep learning models. Hence, we set the quality evaluation threshold as 75%, which means if an image has 75% or more absence of positive pixels (the background is regarded as negative), this image is deemed as of poor quality and is discarded from the training dataset. Although, in terms of inputs, our collected shoeprint images are not from real crime scenes, but they are quite similar in various aspects. For instance, the collected dataset comprises abrasive, scratched, noisy, partial, and incomplete shoeprint images which show similarities with the foot impressions found in real scenarios. Thus, by training the proposed model with the collected dataset, it may provide great help in real forensic investigations. Specifically, the model predicts a suspect's age and identifies the gender, which will save much time and resources of the investigators by screening the suspects based on the estimated age and predicted gender. In this way, we preserve the integrity of the trained model. Because our study is the first attempt in the machine learning aspect contributing a large-size shoeprint dataset, we provide the necessary groundwork and hope other researchers will join us to make more contributions along this line together in the near future.

A wide range of experiments were carried out by training different machine-learning models to capture human gait and standing patterns related to aging (Table 4). Some of the trained networks are unable to capture gait patterns. For instance, age prediction from the left or right shoeprints alone could not predict age accurately, as it may not capture much information about walking, standing and wear effects with diverse types of shoes, body weights, etc. In contrast, the proposed ShoeNet model trains on pair-wise shoeprints, and effectively captures features reflecting physical changes that appear with aging. This may indicate that age-related features are mostly reflected in the asymmetric differences between left and right shoeprints. ShoeNet adapts a deep convolutional neural network [28,70] featuring extraction, and its architecture is designed to retain the pressure distribution varying with biological traits pertinent to aging, as well as the distribution differences between L&R shoeprints. Another challenge of this study is a lack of consistent textual-outsole patterns in shoeprints with diverse types of shoes. ShoeNet utilizes pairwise shoeprints to fine-tune the network comprehensively and to capture areas of interest like scratches, cuts and abrasions with gait and standing patterns. ShoeNet retains morphological representations at a deep level capturing age related information, as well meaningful differences between left and right shoeprints related to aging. The significance of ShoeNet design can be reflected in the comparative scores against the SOTA and deep learning customized modalities. The model enabled to extract features at multiple deep levels and merge precisely to correlate with human biological profile. Useful information pass among the blocks with both input and direct connections. Hence, in a wide range of practices, ShoeNet outperformed most SOTA and possible network modalities trained on the given datasets.

To explore aging effects on shoeprints in more detail, we grouped the subjects into a total of five age groups (Table 5 (Type-B)). Each group shows discrepant results for shoeprint-based age prediction. The subjects in the age group of 21–30 years old have the most consistent pressure distribution on shoeprints reflecting the robust association of age to gait and standing patterns while the rest of the subjects vary more due to body and health conditions. As in real crime scenes, mostly the offenders were found around the age of 25 years [71], where the age prediction is more accurate for the age group 21–30 years (Table 5). This extrapolates the relative association of pressure distribution of collected samples with that of crime scenes statistics.

The human body morphological effects on shoeprints can be illustrated in the form of a pressure-spreading anatomy (Fig. 5). To extrapolate the pressure trends precisely, we superimposed the shoeprint images category wise (e.g., 21–30, 31–40, and so on). For superimposition, we transformed the length and width of shoeprint impressions into the same standard. However, the shoeprints are not standardized in terms of length and width for the subsequent training and testing processes. The most obvious pressure trends were found spreading from the interior to exterior regions over aging. In particular, the pressure trends increase up to 40 years old and then a steady decline is observed which was reflected in regions R_0 , R_2 , R_3 and R_5 (Fig. 6(a, b)). Previous studies have shown that abrasion points occur with the specific pressure of foot-muscles on certain areas of shoeprints while in contact with the ground surface [37,50]. Our study provides evidence for such intensive forces on shoeprints with the depiction of pressure trends (Figs. 6 and 8). We also expanded the frontier of gender-based wear effects on shoeprints in the capacity of pressure distributions (Fig. 8), which may assist in a wide range of fields, especially forensic podiatry. These pressure distribution trends are distinct from one age group to another. After age prediction and gender classification, further evidence, identification, and confirmation of a suspect demographic (age, gender etc.) can be carried out by pressure trends examination. Thus, the examination of pressure distribution trends in the acquired digital shoeprint provides a decision support to investigators to find out strong association to a particular age-group and gender-class. Similarly, in earlier studies, shoeprint-based gender predictions were carried out from morphological features (like shoeprint length and width) and via regression by using hand-crafted features [39,72,73], while ShoeNet adopts convolution filters for feature extraction from the pictures of shoeprints directly for the end-to-end gender prediction (86.07%) in the large-scale balanced dataset (Table 6). We can observe that the males and females have distinct pressure distributions in terms of intensity values, trend patterns, and age growing fluctuations in the corresponding regions. Evidently, males have higher pressure trends except for the outer front toes of both L&R shoeprints (region R_0) (Fig. 8(a and b)). The high gender classification accuracy (86.07%) also confirms study findings about gait pattern variations between males and females [44]. Taken together, ShoeNet exploits varying effects in distinct age groups and achieves good result for age estimation and gender prediction. This study will provide useful information and methods for forensic investigations, gait-pattern disorders associated with aging, and biological profile estimations, as well as sports and clinical investigations. Most importantly, the predicted traits including height, age, and sex will increase the chances to narrow down suspects in the crime scenes.

4. Future directions

This study is the first machine/deep learning based attempt to estimate human age and gender-sex from a pairwise shoeprint which can be extended to other biological profiles prediction (height, weight, ethnicity, etc.). Moreover, asymmetric features extraction from pair-wise and the variations between left to right shoeprint images can be explored into a worthy outcome by associating to a person walking style. The walking style can further be utilized for the suspect identity in the field of forensic science. Furthermore, for the training of a reconstruction model, ground truth images are rarely available, hence, the asymmetric features between left and right shoeprint can be jointly used for shoeprint image reconstruction. Our current study aims to predict the age and gender based on the shoeprints that could be found in real forensic scenes, therefore, it is not necessary that shoes must be classified as jogger, heel, etc. In addition to age prediction, we also classified the shoe impressions based on gender. By gender we mean male and

female only; however, the transgender option may be added in the future study. As a possible extension of our current study, more shoeprints of a larger variety of the shoe types can be collected, so that different classes of footwear can be separately studied and possibly classified together with their association to human demographic. By discarding the poor quality images and retaining the integrity of a reliable deep learning model, we believe that one of the promising future research directions is to tolerate training data with inferior quality. Deep learning models can also be applied to shoeprint enhancement, super-resolution, reconstruction of abrasion, and generation of complete shoeprint as demanded in forensic science. We provide the necessary groundwork and hope other researchers will join us to make more contributions along this line together in the near future.

Authors contributions

Muhammad Hassan contributed to the theoretical development, experimental design, and prototype development. Prepared the datasets for network training and evaluation, designed and tuned the network model, trained and validated the ShoeNet model. Furthermore, Muhammad Hassan evaluated the findings against SOTA models and analyzed the association to the realistic scenario. Finally, proceeded the findings into documentation in the form of paper writing. Yan Wang made significant contributions to experimental design, prototype development, methodology, results analysis and gave a proofreading and critical revision of the article. Yan Wang also contributed to carry out the state-of-the-art studies and comparison. Di Wang contributed to the model design, parameters selection, and the interpretation of findings and validation. Di Wang revised the draft and approved the final version for submission. Daixi Li contributed to the collection of shoeprint samples from subjects and data curation. Daixi Li also interpreted the data associated with the current study. Yanchun Liang analyzed, interpreted the datasets, and revised the paper writing as proofreading. Yanchun Liang also directed to perform the qualitative and quantitative comparison and analysis against the state-of-the-art models. You Zhou supervised and directed the whole procedure, assisted in prototyping the developmental process, analyzed and interpreted the associated data in the study. You Zhou performed proofreading and critical revision of the article. Dong Xu supervised and directed the whole study, encouraged to carry out various experimental designs, analysis, result evaluations, and contributed to the final draft with proofreading and approval of the version to be submitted.

Code availability

The code and related documents are available on <https://github.com/mhassandev/ShoeNet>.

Data availability

All the initial datasets were collected via the EverOS V2.0 acquisition system by Everspray Science and Technology Company Ltd., Dalian, China, and the rest of the dataset versions were generated by manual and automatic processing. All the datasets are available to the research community following the terms and conditions set forth at http://www.everspray.com/en/service/data_open.html.

Declaration of Competing Interest

The authors declare that they have no known competing financial interests or personal relationships that could have appeared to influence the work reported in this paper.

Acknowledgment

This research is supported by the National Natural Science Foundation of China (Grants Nos. 61772227, 61972174, 61972175), Science and Technology Development Foundation of Jilin Province (No. 20180201045GX, 20200201300JC, 20200401083GX, 20200201163JC), and the Jilin Development and Reform Commission Fund (No. 2020C020-2), as well as the Paul K. and Diane Shumaker Endowment Fund to DX. We like to thank Ms. Carla Roberts for thoroughly proofreading this paper.

Appendix A. Supporting information

Supplementary data associated with this article can be found in the online version at doi:[10.1016/j.forsciint.2021.110987](https://doi.org/10.1016/j.forsciint.2021.110987).

References

- [1] I. Rida, Towards human body-part learning for model-free gait recognition, arXiv preprint arXiv:1904.01620.
- [2] W. Rowe, Interpretation of shoe wear patterns in a personal injury case, *J. Forensic Sci.* 26 (1981) 608–611.
- [3] T. Fruchtenicht, W. Herzig, R.D. Blackledge, The discrimination of two-dimensional military boot impressions based on wear patterns, *Sci. Justice* 42 (2002) 97–104.
- [4] S.N. Srihari, Analysis of footwear impression evidence, final technical report, award number: 2007-dn-bx-k135, awarded to research foundation of the state university of new york, US Dpartment of Justice Report.
- [5] W.J. Bodziak, *Footwear Impression Evidence: Detection, Recovery and Examination*, CRC Press, 1999.
- [6] G. Alexandre, Computerized classification of the shoeprints of burglars' soles, *Forensic Sci. Int.* 82 (1996) 59–65.
- [7] Z. Geraarts, J. Keijzer, The image-database rebezo for shoeprints with developments on automatic classification of shoe outsole designs, *Forensic Sci. Int.* 82 (1996) 21–31.
- [8] I. Rida, N. Al-Maadeed, S. Al-Maadeed, S. Bakshi, A comprehensive overview of feature representation for biometric recognition, *Multimed. Tools Appl.* (2018) 1–24.
- [9] M. Acevedo Mosqueda, M. ACEVEDO MOSQUEDA, R. Carreno Aguilera, F. Martínez Zuñiga, D. Pacheco Bautista, M. Patiño Ortiz, W. Yu, Computational intelligence for shoeprint recognition, *Fractals* 27 (04) (2019) 1950080.
- [10] Y. Zhang, H. Fu, E. Dellandréa, L. Chen, Adapting convolutional neural networks on the shoeprint retrieval for forensic use, in: Chinese Conference on Biometric Recognition, Springer, 2017, pp. 520–527.
- [11] X. Francis, H. Sharifzadeh, A. Newton, N. Baghaei, S. Varastehpour, Learning wear patterns on footwear outsoles using convolutional neural networks, in: 2019 18th IEEE International Conference on Trust, Security and Privacy on Computing and Communications/13th IEEE International Conference on Big Data Science and Engineering (TrustCom/BigDataSE), IEEE, pp. 450–457.
- [12] Z. Ma, Y. Ding, S. Wen, J. Xie, Y. Jin, Z. Si, H. Wang, Shoe-print image retrieval with multi-part weighted cnn, *IEEE Access* 7 (2019) 59728–59736.
- [13] J. Cui, X. Zhao, N. Liu, S. Morgachev, D. Li, Robust shoeprint retrieval method based on local-to-global feature matching for real crime scenes, *J. Forensic Sci.* 64 (2019) 422–430.
- [14] B. Kong, J. Supancic, D. Ramanan, C. Fowlkes, Cross-domain forensic shoeprint matching.
- [15] K. Simonyan, A. Zisserman, Very deep convolutional networks for large-scale image recognition, arXiv preprint arXiv:1409.1556.
- [16] S. Krig, *Interest point detector and feature descriptor survey*, *Computer Vision Metrics*, Springer, 2016, pp. 187–246.
- [17] I. Rida, S. Bakshi, H. Proenca, L. Fei, A. Nait-Ali, A. Hadid, Forensic shoe-print identification: a brief survey, arXiv preprint arXiv:1901.01431.
- [18] Y. Tang, S.N. Srihari, H. Kasiviswanathan, J.J. Corso, Footwear print retrieval system for real crime scene marks, in: International Workshop on Computational Forensics, Springer, 2010, pp. 88–100.
- [19] N. Basu, S.K. Bandyopadhyay, Crime scene reconstruction-sex prediction from blood stained foot sole impressions, *Forensic Sci. Int.* 278 (2017) 156–172.
- [20] E.A. Okubike, M.E. Nandi, E.C. Iheaza, O.C. Obun, Stature prediction using shoe print dimensions of an adult nigerian population, *Arab J. Forensic Sci. Forensic Med.* 1 (2019) 989–1003.
- [21] H. Ozden, Y. Balci, C. Demir, A. Turgut, M. Ertugrul, Stature and sex estimate using foot and shoe dimensions, *Forensic Sci. Int.* 147 (2005) 181–184.
- [22] D. Atamturk, Estimation of sex from the dimensions of foot, footprints, and shoe, *Anthropol. Anz.* (2010) 21–29.
- [23] R. Xiao, P. Shi, Computerized matching of shoeprints based on sole pattern, in: International Workshop on Computational Forensics, Springer, 2008, pp. 96–104.
- [24] D. Cunado, M.S. Nixon, J.N. Carter, Automatic extraction and description of human gait models for recognition purposes, *Comput. Vis. Image Underst.* 90 (2003) 1–41.

- [25] J. Han, B. Bhanu, Individual recognition using gait energy image, *IEEE Trans. Pattern Anal. Mach. Intell.* 28 (2005) 316–322.
- [26] M.P. Murray, Gait as a total pattern of movement: Including a bibliography on gait, *Am. J. Phys. Med. Rehabil.* 46 (1967) 290–333.
- [27] M.P. Murray, A.B. Drought, R.C. Kory, Walking patterns of normal men, *JBJS* 46 (1964) 335–360.
- [28] L. Marado, J. Ribeiro, Biological profile estimation based on footprints and shoemarks from bracara augusta figlineae (brick workshops), *Heritage* 1 (2018) 33–44.
- [29] T.D. White, P.A. Folkens, Human Osteology, Gulf Professional Publishing, 2000.
- [30] V. Novotný, Morphologic and osteometric assessment of age, sex, and race from the skull, *Forensic Analysis of the Skull: Craniofacial Analysis, Reconstruction, and Identification*, 1993, pp. 71–88.
- [31] R. Angulu, J.R. Tapamo, A.O. Adewumi, Age estimation via face images: a survey, *EURASIP J. Image Video Process.* 2018 (2018) 42.
- [32] Y. Wang, M. Kosinski, Deep neural networks are more accurate than humans at detecting sexual orientation from facial images, *J. Personal. Soc. Psychol.* 114 (2018) 246.
- [33] B. Jonsson, G. Björnsdóttir, T. Thorgeirsson, L. Ellingsen, G.B. Walters, D. Gudbjartsson, H. Stefansson, K. Stefansson, M. Ólafsson, Brain age prediction using deep learning uncovers associated sequence variants, *Nat. Commun.* 10 (2019) 1–10.
- [34] N. Pardakhteh, H. Sajedi, Age prediction based on brain mri images using feature learning, in: 2017 IEEE 15th International Symposium on Intelligent Systems and Informatics (SISY), IEEE, 2017, pp. 000267–000270.
- [35] O. Al Zoubi, C. Ki Wong, R.T. Kuplicki, H.-w. Yeh, A. Mayeli, H. Refai, M. Paulus, J. Bodurka, Predicting age from brain eeg signals – a machine learning approach, *Front. Aging Neurosci.* 10 (2018) 184.
- [36] X. Li, W. Li, Y. Xu, Human age prediction based on dna methylation using a gradient boosting regressor, *Genes* 9 (2018) 424.
- [37] A. Abutorabi, M. Arazpour, M. Bahramizadeh, S.W. Hutchins, R. Fadavayatan, The effect of aging on gait parameters in able-bodied older subjects: a literature review, *Aging Clin. Exp. Res.* 28 (2016) 393–405.
- [38] Y. Makihara, H. Mannami, Y. Yagi, Gait analysis of gender and age using a large-scale multi-view gait database, in: Asian Conference on Computer Vision, Springer, 2010, pp. 440–451.
- [39] D.S. Ekezie, J. Ndubuka, G.I. Oji, Okeke SN, A study of correlations and estimation of stature from foot trace and shoe trace dimensions, *Int. J. Forensic Sci.* 1 (2016) 1–8.
- [40] L. Alcock, N. Vanicek, T. O'Brien, Alterations in gait speed and age do not fully explain the changes in gait mechanics associated with healthy older women, *Gait Posture* 37 (2013) 586–592.
- [41] N. Alexander, Gait disorders in older adults, *J. Am. Geriatr. Soc.* 44 (1996) 434–451.
- [42] W. Pirker, R. Katzenzchlager, Gait disorders in adults and the elderly, *Wien. Klin. Wochenschr.* 129 (2017) 81–95.
- [43] S. Studenski, S. Perera, K. Patel, C. Rosano, K. Faulkner, M. Inzitari, J. Brach, J. Chandler, P. Cawthon, E.B. Connor, et al., Gait speed and survival in older adults, *JAMA* 305 (1) (2011) 50–58.
- [44] M.M. Samson, A. Crowe, P. De Vreede, J.A. Dessens, S.A. Duursma, H.J. Verhaar, Differences in gait parameters at a preferred walking speed in healthy subjects due to age, height and body weight, *Aging Clin. Exp. Res.* 13 (2001) 16–21.
- [45] B.E. Maki, Gait changes in older adults: predictors of falls or indicators of fear? *J. Am. Geriatr. Soc.* 45 (1997) 313–320.
- [46] N.-M. Yoon, H.-J. Yoon, J.-S. Park, H.-S. Jeong, G. Kim, The comparative study on age-associated gait analysis in normal korean, *J. Korean Phys. Ther.* 22 (2010) 15–23.
- [47] R.L. Waters, S. Mulroy, The energy expenditure of normal and pathologic gait, *Gait Posture* 9 (1999) 207–231.
- [48] P.M. Coen, S.A. Jubrias, G. Distefano, F. Amati, D.C. Mackey, N.W. Glynn, T.M. Manini, S.E. Wohlgemuth, C. Leeuwenburgh, S.R. Cummings, et al., Skeletal muscle mitochondrial energetics are associated with maximal aerobic capacity and walking speed in older adults, *J. Gerontol. Ser. A: Biomed. Sci. Med. Sci.* 68 (4) (2013) 447–455.
- [49] R.W. Bohannon, A.W. Andrews, Normal walking speed: a descriptive meta-analysis, *Physiotherapy* 97 (2011) 182–189.
- [50] M. Lord, D.P. Reynolds, J.R. Hughes, Foot pressure measurement: a review of clinical findings, *J. Biomed. Eng.* 8 (1986) 283–294.
- [51] E.L. Radin, Osteoarthritis. what is known about prevention, *Clin. Orthop. Relat. Res.* (1987) 60–65.
- [52] M.W. Whittle, Generation and attenuation of transient impulsive forces beneath the foot: a review, *Gait Posture* 10 (1999) 264–275.
- [53] M. Kuhn, K. Johnson, et al., *Applied Predictive Modeling*, 26 Springer, 2013.
- [54] J. Brownlee, Data preparation for machine learning: data cleaning, feature selection, and data transforms in Python, *Mach. Learn. Master* (2020).
- [55] S. Suzuki, et al., Topological structural analysis of digitized binary images by border following, *Comput. Vis. Graph. Image Process.* 30 (1) (1985) 32–46.
- [56] B. Nickerson, P. Fitzhorn, S. Koch, M. Charney, A methodology for near-optimal computational superimposition of two-dimensional digital facial photographs and three-dimensional cranial surface meshes, *J. Forensic Sci.* 36 (1991) 480–500.
- [57] W. Aulsebrook, M. İşcan, J. Slabbert, P. Becker, Superimposition and reconstruction in forensic facial identification: a survey, *Forensic Sci. Int.* 75 (1995) 101–120.
- [58] P. Jayaprakash, B. Singhb, R. Yusopc, H. Susilawati, Skull-photo superimposition: a remedy to the problem of unidentified dead in malaysian, *Malays. J. Forensic Sci.* 1 (2010) 35–42.
- [59] L. Glass, Moire effect from random dots, *Nature* 223 (1969) 578–580.
- [60] M.G. Donaldson, B. Sobolev, L. Kuramoto, W.L. Cook, K.M. Khan, P.A. Janssen, Utility of the mean cumulative function in the analysis of fall events, *J. Gerontol. Ser. A: Biol. Sci. Med. Sci.* 62 (2007) 415–419.
- [61] A. Zemla, Lga: a method for finding 3d similarities in protein structures, *Nucleic Acids Res.* 31 (2003) 3370–3374.
- [62] M. Viljanen, A. Airola, A.-M. Majanoja, J. Heikkonen, T. Pahikkala, Measuring player retention and monetization using the mean cumulative function, *IEEE Trans. Games* 12 (2020) 101–114.
- [63] K. He, X. Zhang, S. Ren, J. Sun, Deep residual learning for image recognition, in: Proceedings of the IEEE Conference on Computer Vision and Pattern Recognition, 2016, pp. 770–778.
- [64] G. Huang, Z. Liu, L. Van Der Maaten, K.Q. Weinberger, Densely connected convolutional networks, in: Proceedings of the IEEE Conference on Computer Vision and Pattern Recognition, 2017, pp. 4700–4708.
- [65] R.K. Srivastava, K. Greff, J. Schmidhuber, Highway networks, arXiv preprint arXiv:1505.00387.
- [66] A. Krizhevsky, I. Sutskever, G.E. Hinton, Imagenet classification with deep convolutional neural networks, in: Advances in Neural Information Processing Systems, 2012, pp. 1097–1105.
- [67] C. Szegedy, W. Liu, Y. Jia, P. Sermanet, S. Reed, D. Anguelov, D. Erhan, V. Vanhoucke, A. Rabinovich, Going deeper with convolutions, in: Proceedings of the IEEE Conference on Computer Vision and Pattern Recognition, 2015, pp. 1–9.
- [68] C. Szegedy, S. Ioffe, V. Vanhoucke, A.A. Alemi, Inception-v4, inception-resnet and the impact of residual connections on learning, in: Thirty-first AAAI Conference on Artificial Intelligence, 2017.
- [69] R. Angulu, J.R. Tapamo, A.O. Adewumi, Age estimation via face images: a survey, *EURASIP J. Image Video Process.* 2018 (2018) 42.
- [70] L. Nanni, S. Ghidoni, S. Brahnam, Handcrafted vs. non-handcrafted features for computer vision classification, *Pattern Recognit.* 71 (2017) 158–172.
- [71] M. Rocque, C. Posick, J. Hoyle, Age and crime, *The encyclopedia of crime and punishment*, 2015, pp. 1–8.
- [72] C.C. Gordon, J.E. Buikstra, Linear models for the prediction of stature from foot and boot dimensions, *J. Forensic Sci.* 37 (1992) 771–782.
- [73] D. Atamtürk, I. Duyar, Age-related factors in the relationship between foot measurements and living stature and body weight, *J. Forensic Sci.* 53 (2008) 1296–1300.